Boletim da Sociedade Astronômica Brasileira, **31**, no. 1, 48-50

Mapping the accretion disc of the short period eclipsing binary SDSS J0926+3624

W. Schlindwein[1] & R. Baptista[1]

[1] Universidade Federal de Santa Catarina
e-mail: wagner.schlindwein@astro.ufsc.br, raybap@gmail.com

Abstract. We observed SDSS J0926+3624 with the Liverpool Robotic Telescope between 2012 February-March while the object was in its quiescent brightness state. We combined our median eclipse timing with those in the literature to revise the ephemeris and confirm that the binary period is increasing at a rate $\dot{P} = (3.2 \pm 0.4) \times 10^{-13}\, s/s$. We applied eclipse mapping techniques to the average light curve to map the surface brightness distribution of the accretion disc. The eclipse map shows a hot white dwarf surrounded by a faint, cool accretion disc plus enhanced emission along the gas stream trajectory beyond the impact point at the outer disc rim, suggesting the occurrence of gas stream overflow/penetration at that epoch. Moreover, we estimate a disc mass input rate of $\dot{M} = (9 \pm 1) \times 10^{-12}\, M_\odot\, yr^{-1}$, more than an order of magnitude lower than that expected from binary evolution with conservative mass transfer.

Resumo. Nós observamos SDSS J0926+3624 com o Telescópio Robótico Liverpool entre fevereiro-março de 2012 quando o objeto estava no seu estado quiescente de brilho. Combinamos nosso tempo de eclipse médio com os da literatura para revisar as efemérides e confirmamos que o período da binária está aumentando a uma taxa de $\dot{P} = (3.2 \pm 0.4) \times 10^{-13}\, s/s$. Aplicamos a técnica de mapeamento por eclipse na curva de luz média para mapear a distribuição superficial de brilho do disco de acréscimo. O mapa de eclipse mostra uma anã branca quente cercada por um disco de acréscimo fraco e frio, mais uma emissão aumentada ao longo da trajetória do fluxo de gás para além do ponto de impacto na borda externa do disco, sugerindo a ocorrência de transbordamento/penetração do fluxo de gás nessa época. Além disso, estimamos uma taxa de entrada em massa no disco de $\dot{M} = (9 \pm 1) \times 10^{-12}\, M_\odot\, yr^{-1}$, mais do que uma ordem de magnitude menor do que a esperada pela evolução binária com transferência de massa conservativa.

Keywords. Stars: dwarf novae – binaries: eclipsing – novae, cataclysmic variables

1. Introduction

AM Canum Venaticorum (AM CVn) stars are ultracompact binaries ($P_{orb} < 65$ min) where a hidrogen-deficient low-mass, degenerate donor star overfills its Roche lobe and transfers matter to a companion white dwarf via an accretion disc (see e.g. Nelemans 2005; Ramsay et al. 2007; Roelofs et al. 2010). SDSS J0926+3624 (hereafter J0926) is currently the only eclipsing AM CVn star and also one of the shortest period eclipsing binary known (Anderson et al. 2005). Its light curve displays deep (~ 2 mag) eclipses every 28.3 min, which last for ~ 2 min, as well as ~ 2 mag amplitude outbursts every $\sim 100 - 200$ d (Copperwheat et al. 2011). Superhumps were seen in its light curves several days after the end of an outburst (Copperwheat et al. 2011; Szypryt et al. 2014); these are believed to result from the tidal interaction between the mass-donor star and an elliptical precessing disc (e.g., Whitehurst 1988; Hirose & Osaki 1990).

Copperwheat et al. (2011) modeled the eclipse light curves to estimate masses and radii of both stars, a mass ratio $q = M_2/M_1 = 0.041 \pm 0.002$ and an inclination $i = 82.^\circ6 \pm 0.^\circ3$, a white dwarf temperature of $T_{wd} = 17000\, K$ and a corresponding distance estimate of (465 ± 5) pc. Szypryt et al. (2014) found that the orbital period of J0926 is increasing at a rate $\dot{P} = (3.07 \pm 0.56) \times 10^{-13}\, s/s$ and, as a consequence, inferred a conservative mass transfer rate $\dot{M} \simeq 1.8 \times 10^{-10}\, M_\odot\, yr^{-1}$. This is in agreement with the $\dot{M} = (1.4 \pm 0.3) \times 10^{-10}\, M_\odot\, yr^{-1}$ predicted by Deloye et al. (2007) based on their stellar evolutionary calculations (corrected for the $q = 0.041$ value of Copperwheat et al. 2011).

2. Analysis and results

J0926 was observed with the 2.0 m Liverpool Robotic Telescope in 2014 February-March using the $V + R$ passband of the RISE camera when it was in the quiescent brightness state and near the end of a 4.6 yr long period without recorded outbursts. The data cover 20 binary orbits. The complete data reduction procedure is described in Section 2 of Schlindwein & Baptista (2018).

The individual light curves were phase-folded according to the linear ephemeris of Copperwheat et al. (2011),

$$T_{\rm mid}({\rm BJDD}) = 2\,453\,796.445\,5191(5) + 0.019\,661\,272\,89(2) \times E \quad , (1)$$

where $T_{\rm mid}$ is the primary mid-eclipse time and E is the binary cycle. As the average light curves of all nights show the same morphology, brightness level, eclipse shape and depth, we combined all data to obtain a single average light curve with increased S/N.

We used a phase-folded, concatenated light curve to obtain a single mid-eclipse time from the whole data set, and we obtain a value of $T_{\rm mid}(E = 112\,505) = {\rm BJDD}\ 2\,456\,008.437\,044(10)$ for the equivalent observed mid-eclipse timing. We combined our timing with those in the literature to review the J0926 ephemeris. The results are listed in Table 2 of Schlindwein & Baptista (2018). Table 1 presents the parameters of the best-fit linear and quadratic ephemerides to these timings with their 1-σ formal errors quoted, together with the root-mean-square value of the residuals, σ, and the reduced χ^2_ν, where ν is the number of degrees of freedom. These fits assume equal errors of $2.2 \times 10^{-6}\, d$ to the data points, which ensures a unity χ^2_ν for the quadratic ephemeris. The significance of adding an additional term to the linear ephemeris was estimated with the F-test (Pringle 1975).

Table 1: Ephemerides for mid-eclipse times of J0926. [a]

Linear ephemeris:	
BJDD = $T_0 + P_0\,E$	
T_0 = 2 453 796.445 510(±1) d	P_0 = 0.019 661 273 12(±2) d
$\chi^2_{\nu_1}$ = 9.56 , ν_1 = 6	$\sigma_1 = 6.23 \times 10^{-6}\,d$
Quadratic ephemeris:	
BJDD = $T_0 + P_0\,E + c\,E^2$	
T_0 = 2 453 796.445 514(±1) d	P_0 = 0.019 661 272 75(±5) d
$c = (+3.18 \pm 0.44) \times 10^{-15}\,d$	$\sigma_2 = 1.85 \times 10^{-6}\,d$
$\chi^2_{\nu_2}$ = 1.00 , ν_2 = 5	

[a] Reprinted with permission from Schlindwein & Baptista (2018).

The quadratic ephemeris has a statistical significance of 99.9 per cent with $F(1,6) = 51.7$.

The orbital period of J0926 seems to be increasing at a rate $\dot{P} = (3.24 \pm 0.43) \times 10^{-13}\ s/s$, and this value is consistent with that found by Szypryt et al. (2014) within the uncertainties. According to Szypryt et al. (2014), this increase could possibly be the consequence of binary evolution through angular momentum loss caused by gravitational radiation. However, given that every eclipsing cataclysmic variables with a well-sampled (O-C) diagram covering at least a decade of observations shows cyclical period changes (e.g., Borges et al. 2008), the observed period increase could alternatively be part of a cyclical period modulation of amplitude several seconds on a decade long timescale. Given the precision with which eclipses can be measured in this binary, a further decade of (regular) observations will suffice to clarify these possibilities.

We searched for periodicities in the light curves by computing a Lomb-Scargle periodogram (Press et al. 1992) for each separate night, but the periodograms show no prominent signal at orbital ($f_{\rm orb} = 50.9\,d^{-1}$), superhump ($f_{\rm sh} = 50.4\,d^{-1}$, Copperwheat et al. 2011), or at any other frequency in the range $f < 2000\,d^{-1}$.

We applied eclipse mapping techniques (Horne 1985; Baptista 2016) to the average light curve of J0926 to obtain the disc brightness distribution and the flux of an additional uneclipsed component.

Our eclipse map is a flat Cartesian grid of 51 × 51 pixels centered on the primary star with side $2R_{L_1}$ (where R_{L_1} is the distance from the disc center to the inner Lagrangian point). The eclipse geometry is defined by the mass ratio q and the inclination i. We adopted the parameters of Copperwheat et al. (2011), $R_{L_1} = (0.231 \pm 0.009)\,R_\odot$, $q = 0.041 \pm 0.002$ and $i = 82.6° \pm 0.03°$, which correspond to a white dwarf (WD) eclipse phase width of $\Delta\phi = 0.022$. This combination of parameters ensures that the WD is at the center of the map.

Our eclipse mapping code implements the scheme of double default functions, $D_+\,D_-$, simultaneously steering the solution towards the most nearly axi-symmetric map consistent with the data (D_+), and away from the criss-crossed arcs along the edges of the shadow of the occulting, mass-donor star (D_-) (Spruit 1994; Baptista et al. 2005; Baptista 2016). It is optimized to recover asymmetric structures in eclipse maps such as spiral arms and enhanced gas stream emission. The positive default function is a polar Gaussian with radial and azimuthal blur widths of $\Delta r = 0.02\,R_{L_1}$ and $\Delta\theta = 30°$, respectively. The negative default function is a Gaussian along the ingress/egress arcs of phase width $\Delta\phi = 0.01$.

We model the contribution of the WD from the ecplise geometry assuming a DB white dwarf with $M_{WD} = 0.85\,M_\odot$, $\log g = 8.33$, $T_{WD} = 17000\,K$ and a distance of 465 pc (Copperwheat et al. 2011), taking into account the effects of limb darkening (Gianninas et al. 2013).

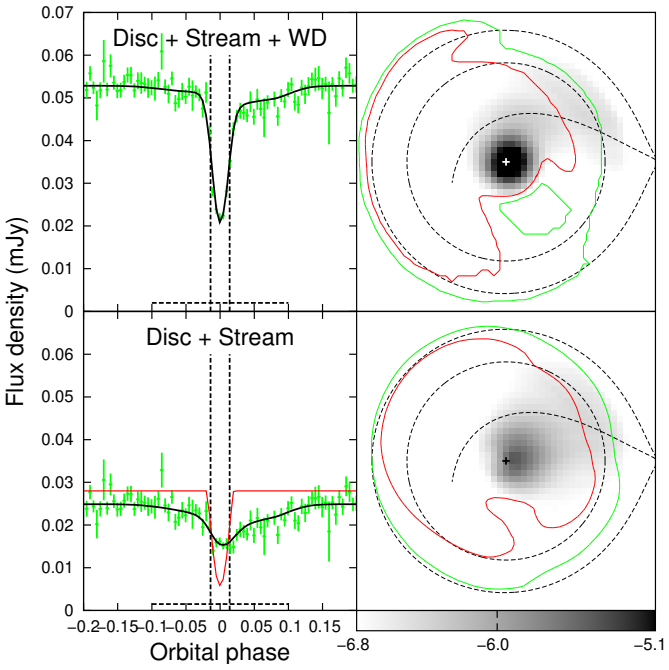

Figure 1: *Upper left panel:* Data (green crosses with error bars) and model (black line) light curves. *Lower left panel:* WD-subtracted data (green crosses with error bars) and model (black line) light curves. The red solid line depicts the model WD eclipse light curve. Horizontal dashed lines indicate the uneclipsed flux in each panel. Vertical dashed lines mark the ingress/egress phases of the WD. *Upper right panel:* Surface brightness distribution of the combined disc+stream+WD map in a logarithmic grayscale. *Lower right panel:* WD-subtracted surface brightness distribution. Regions inside the green/red contour lines are above the 2- and 3-σ confidence levels, respectively. Dashed lines depict the primary Roche lobe, a disc of radius $0.65\,R_{L_1}$, and the ballistic stream trajectory. The horizontal bar shows the logarithmic intensity grayscale; brighter regions are darker (Reprinted with permission from Schlindwein & Baptista 2018).

The results of the application of eclipse mapping techniques on data without/with WD-subtracted are shown in the upper/lower panel of Fig. 1. The statistical uncertainties in the eclipse maps are estimated with a Monte Carlo procedure (see e.g. Rutten et al. 1992), using a set of 10^2 artificial curves in which the data points are independently and randomly varied according to a Gaussian distribution with standard deviation equal to the uncertainty at that point.

The upper panel of Fig. 1 displays the eclipse map of the full light curve. The brightness distribution is dominated by the contribution from the WD at disc center. Aside of the deep, narrow eclipse of the WD, the additional broad, shallow and asymmetric eclipse shape maps into two asymmetric brightness sources, one running along the disc rim at $R_d \simeq 0.65\,R_{L_1}$ (signalling the presence of a weak bright spot), and the other extending along the ballistic stream trajectory beyond the impact point at disc rim (suggesting the presence of gas stream overflow/penetration). The fact that this residual bright spot leads to no perceptible orbital hump in the light curve suggests that at least the outer disc regions are optically thin. The lower panel shows the WD-subtracted light curve and corresponding eclipse map, revealing a faint disc at the center of the map as well as the two above mentioned asymmetric sources. These three brightness sources are statistically significant at the 2.5σ (bright spot) and 3-5 σ

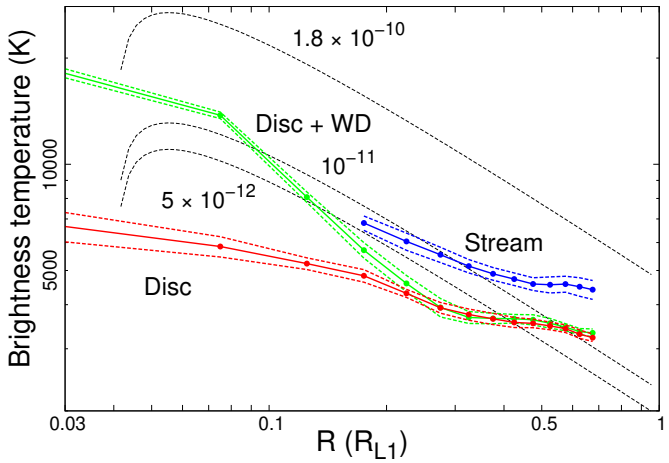

Figure 2: Azimuthally averaged radial brightness temperature distributions for the gas stream ($\theta = 0°-90°$, blue), and for the full ('disc+WD', green) and WD-subtracted ('disc', red) eclipse maps ($\theta = 90° - 360°$) for an assumed distance of 465 pc. The dotted curves show the 1σ limits on the corresponding distributions. Effective temperature distributions of opaque, steady-state disc models for mass accretion rates of $5 \times 10^{-12}, 10^{-11}$, and $1.8 \times 10^{-10}\, M_\odot\, yr^{-1}$ are shown as dotted lines (Reprinted with permission from Schlindwein & Baptista 2018).

(disc plus gas stream emission) confidence levels. We find small and non significant uneclipsed components of 0.002 ± 0.001 mJy for both the full and the WD-subtracted light curves.

We performed simulations in order to gauge the ability of our eclipse mapping code to distinguish between a bright spot at disc rim and extended emission along the ballistic stream trajectory, and these simulations show that the data allow us to easily distinguish between a compact bright spot at disc rim and an extended emission along the stream trajectory (see Fig. 5 of Schlindwein & Baptista 2018).

We assumed a distance of (465 ± 5) pc (Copperwheat et al. 2011) to convert the intensities of the eclipse maps to blackbody brightness temperatures (T_b). Fig. 2 shows the azimutally averaged radial brightness temperature distributions of the combined (disc+stream+WD) and of the WD-subtracted surface brightness distributions. The WD at disc center has $T_b = (19 \pm 1) \times 10^3\, K$, consistent at the 2-$\sigma$ limit with the assumed WD temperature and indicating that $T_b \simeq T_{\rm eff}$ in this case. It is surrounded by a faint, cool accretion disc ($T_b \simeq$ 6000-3500 K in the range 0.1-0.5 R_{L_1}) with enhanced emission along a hotter gas stream ($T_b \simeq$ 7000-4500 K).

From the brightness temperatures in the outer disc regions (R = 0.5-0.6 R_{L1}) we estimate a disc mass input rate of $\dot{M} = (9 \pm 1) \times 10^{-12}\, M_\odot\, yr^{-1}$, more than an order of magnitude lower than the $\dot{M}$ expected from binary evolution with conservative mass transfer ($\simeq 1.8 \times 10^{-10}\, M_\odot\, yr^{-1}$, Szypryt et al. 2014).

We put forward a few possible explanations for this discrepancy. It may be that the outer disc is optically thin and the gas effective temperatures (and corresponding $\dot{M}$ values) are significantly larger than the inferred T_b values; multicolour (or spectral) eclipse mapping would be helpful to clarify this issue. It may also be that the observed period increase is not a consequence of evolution with conservative mass transfer, but part of a cyclical period change which could hide a long term period increase at a much slower pace (a $\dot{P} \sim 1.5 \times 10^{-14}\, s/s$ would be expected from the above mass transfer rate estimate). A third explanation would be that the present mass transfer rate of J0926 is significantly lower than its secular average. This raises the possibility of the existence of large amplitude, long-term modulations in mass transfer rates of AM CVn stars similar to those which presumably occur in cataclysmic variables (the hibernation scenario of novae, see Kovetz et al. 1988). However, while in CVs these modulations seem a consequence of their recurrent nova eruptions, in AM CVn stars a different mechanism would be required since their hydrogen-deficient discs cannot drive hydrogen-burning thermonuclear runaways at the WD surface.

3. Conclusion

Our study reveals that J0926 was observed close to the end of a 4.6 yr long interval without recorded outbursts. Accordingly, we find no evidence for superhumps in our observations. We combined our median eclipse timing with those in the literature to revise the binary ephemeris and to confirm that the orbital period is increasing at a rate $\dot{P} = (3.2 \pm 0.4) \times 10^{-13}\, s/s$. Eclipse mapping of the average light curve shows a hot white dwarf at disc centre surrounded by a faint, cool accretion disc with a residual bright spot (at $R_d \simeq 0.65\, R_{L1}$) and enhanced emission along the ballistic stream trajectory well beyond the disc rim, suggesting the occurence of gas stream overflow or penetration at that epoch. For an assumed distance of 465 pc, the estimated disc mass input rate of $\dot{M} = (9 \pm 1) \times 10^{-12}\, M_\odot\, yr^{-1}$ is more than an order of magnitude lower than that expected from binary evolution with conservative mass transfer.

Acknowledgements. We thank INCT-A/Brazil, CNPq/Brazil and CAPES/Brazil for financial support through scholarships.

References

Anderson, S. F. et al., 2005, AJ, 130, 2230
Baptista, R., Morales-Rueda, L., Harlaftis, E. T., Marsh, T. R., & Steeghs, D. 2005, A&A, 444, 201
Baptista R., 2016, in Astronomy at High Angular Resolution, Astroph. and Space Science Library, eds. H.M.J. Boffin, G. Hussain, J.-P. Berger, L. Schmidtobreick (Springer: Switzerland), p. 155
Borges, B. W., Baptista, R., Papadimitriou, C., & Giannakis, O. 2008, A&A, 480, 481
Copperwheat C. M. et al., 2011, MNRAS, 410, 1113
Deloye, C. J., Taam, R. E., Winisdoerffer, C., & Chabrier, G. 2007, MNRAS, 381, 525
Gianninas, A., Strickland, B. D., Kilic, M., & Bergeron, P. 2013, ApJ, 766, 3
Hirose, M., & Osaki, Y. 1990, PASJ, 42, 135
Horne, K. 1985, MNRAS, 213, 129
Kovetz, A., Prialnik, D., & Shara, M. M. 1988, ApJ, 325, 828
Nelemans, G., 2005, The Astrophysics of Cataclysmic Variables and Related Objects, ASP Conf. Series 330, eds. J.-M. Hameury and J.-P. Lasota (ASP: San Francisco), p. 27
Press, W. H., Teukolsky, S. A., Vetterling, W. T., & Flannery, B. P. 1992, Numerical Recipes in C, (Cambridge Univ. Press: Cambridge), 1992, 2nd ed.
Pringle, J. E. 1975, MNRAS, 170, 633
Ramsay, G. et al., 2007, 15th European Workshop on White Dwarfs, ASP Conf. Series 372, eds. R. Napiwotzki and M. R. Burleigh (ASP: San Francisco), p. 425
Roelofs, G. H. A. et al., 2010, ApJ, 711, L138
Rutten, R. G. M., van Paradijs, J. & Tinbergen, J., 1992, A&A, 260, 213
Schlindwein, W., & Baptista, R. 2018, MNRAS, 478, 3841
Spruit, H. C. 1994, A&A, 289, 441
Szypryt, P., et al. 2014, MNRAS, 439, 2765
Whitehurst, R. 1988, MNRAS, 232, 35